www.MaterialsViews.com

ADVANCED
OPTICAL
MATERIALS
www.advopticalmat.de

COMMUNICATION

An Ultraviolet-to-NIR Broad Spectral Nanocomposite Photodetector with Gain

Rui Dong, Cheng Bi, Qingfeng Dong, Fawen Guo, Yongbo Yuan, Yanjun Fang, Zhengguo Xiao, and Jinsong Huang*

Optical sensing from the ultraviolet (UV) to the near infrared (NIR) range have broad applications including imaging, telecommunications, biomedicine, environmental monitoring and defence sensing.[1–3] It is desirable to have a photodetector with a response spectrum covering a broad spectral range from UV to NIR. However, commercially available solid-state photodetectors have relatively narrow response spectra. For example, silicon photodetectors are only good for the visible/NIR range, while high-end photodetectors made of SiC are generally selected for UV sensing. Organic/polymer photodetectors are attractive low-cost, uncooled candidates under development which can potentially achieve broad-spectrum detection.[4–13] In addition, the small intrinsic carrier concentration in polymer materials and easy engineering of the interfaces provides a unique path to achieve very low noise in polymer-based photodetectors.[1] It is facile to extend the response spectrum of a polymer photodetector into the NIR range by incorporating NIR-absorbing semiconductor materials such as lead sulfide (PbS) quantum dots (QDs).[14,15] In these polymer:QD hybrid photodetectors, the QDs work as sensitizers and the polymers extract/transport the photogenerated charges. The electronic performances of polymer–QD hybrid devices are determined by the energy-level alignments, film morphology, and organic–inorganic interface. Several strategies have been reported to create a close contact between polymers and QDs, which leads to a better hybrid device performance.[9,12,13] Superior NIR-detection performances have also been realized by integrating PbS QDs with C60 fullerite,[16] or making Schottky contacts with aluminium[17] or gold[18] electrodes. It is inspiring that PbS QD-sensitized poly(3-hexylthiophene) (P3HT):[6,6]-phenyl-C61-butyric acid methyl ester (PCBM) materials have been demonstrated for infrared imaging applicaitons by integrating hybrid photodiodes with amorphous silicon active matrix backplanes.[19–22] In addition to the broad response spectrum and low noise, a large quantum efficiency is needed in a sensitive photodetector. A high external quantum efficiency (EQE) of 51% has been reported for a PbS:P3HT:PCBM ternary hybrid

photodetector; the corresponding responsivity and normalized detectivity were 0.5 A/W and 2.3×10^9 Jones, respectively.[19] It is reasonable to anticipate a better detector performance if the photon-to-current conversion efficiency can be further improved.

In this manuscript, we report a PbS-based NIR hybrid photodetector with an EQE above 100% by the integration of zinc oxide (ZnO) QDs to induce a photoconductive gain. The active layer of the photodetector can be prepared by a single cycle of spin-coating. Moreover, the photodetector shows a tenfold higher responsivity than that of commercial SiC and Si photodetectors in the UV–visible range at room temperature.

The structure of the dual-QD hybrid photodetector is presented in **Figure 1**a. The device structure is similar to bulk heterojunction solar cells with indium tin oxide (ITO) and aluminium used as the anode and cathode, respectively. Both PbS and ZnO QDs were introduced into the polymer blends. The PbS QDs in this study were synthesized by a hot-injection technique involving the quick injection of bis(trimethylsilylsulphide) into a hot lead precursor.[21–23] The average diameter of PbS QDs was about 3.3 nm (maximum 3.7 nm), calculated from the absorption curve. Ligand exchange was processed in the solution phase, and the obtained butylamine-capped PbS QDs were dissolved in 1,2-dichlorobenzene (DCB).

ZnO QDs were prepared by the hydrolysis method developed by Pacholski,[24–26] where ZnO QDs are obtained by quickly adding potassium hydroxide solution into zinc acetate methanol solution. The diameter of the ZnO QDs was approximately 5 nm and the obtained ZnO QDs were also dissolved in DCB. The synthesis method is highly reproducible and reliable, and the ZnO QD solution is almost transparent and can be kept at room temperature for more than three weeks.

The polymer blend consists of hole conductor P3HT and electron conductor PCBM which has been extensively studied in an organic solar cell.[27,28] ZnO QDs and PbS QDs were mixed with a P3HT:PCBM polymer blend separately, and then mixed together right before the coating of the quarternary blend films to avoid the aggregation of ZnO and PbS QDs. Solvent and post-thermal annealing were performed in order to obtain an optimized film morphology for better carrier separation and transportation in a polymer matrix (see the Experimental Section for details).

Figure 1b shows the absorbance of as-prepared dual-QD hybrid films measured from 300 nm to 1100 nm. Thanks to the incorporation of ZnO and PbS QDs, the photodetectors have a wide absorption from the UV to the NIR. The absorption

Dr. R. Dong, C. Bi, Dr. Q. Dong, F. Guo,
Dr. Y. Yuan, Dr. Y. Fang, Z. Xiao, Prof. J. Huang
Department of Mechanical and Materials Engineering
University of Nebraska-Lincoln
Lincoln, Nebraska 68588, USA
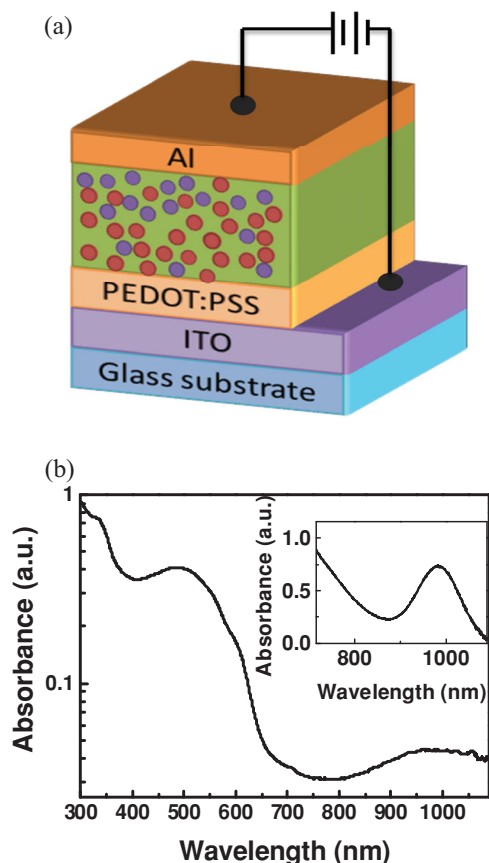E-mail: jhuang2@unl.edu

COMMUNICATION

Figure 1. a) Device structure of the dual-quantum dot hybrid photo-detector. b) Absorption spectrum of the PbS:P3HT:PCBM:ZnO nano-composite films. Inset shows the solution absorbance spectrum of PbS QDs dispersed in toluene.

spectrum of the as-prepared PbS QD solution (dispersed in toluene) is also shown in the inset of Figure 1b.

The influence of the ZnO QDs on the hybrid device is discernible in both photo- and dark-current density (J)-voltage (V) curves of the devices. As shown in **Figure 2**a, the P3HT:PCBM device shows typical photovoltaic characteristics with a 0.6 V open circuit voltage.[27,28] The reverse saturated dark current of the PbS QD- or PbS:ZnO QD-doped P3HT:PCBM devices increased a little bit compared with that of the P3HT:PCBM device, while a clear diode rectifying characteristic is still retained. The photovoltaic effect completely disappears by the incorporation of the PbS and/or ZnO QDs in to P3HT:PCBM because the introduced PbS and/or ZnO QDs act as charge traps, eliminating the photocurrent. The reverse-biased photo-current of the PbS:P3HT:PCBM device is comparable to that of the P3HT:PCBM device, indicating the absence of gain in the devices, which agrees with a previous study.[29] It is notable that the photocurrent of dual-QD hybrid devices is much larger than that of the P3HT:PCBM device as well as that of the PbS:P3HT:PCBM hybrid device, which is clear evidence of photoinduced charge injection.

The presence of a gain in the quaternary blend film device was confirmed by EQE measurements with an incident photon-to-current efficiency (IPCE) system at different reverse biases,
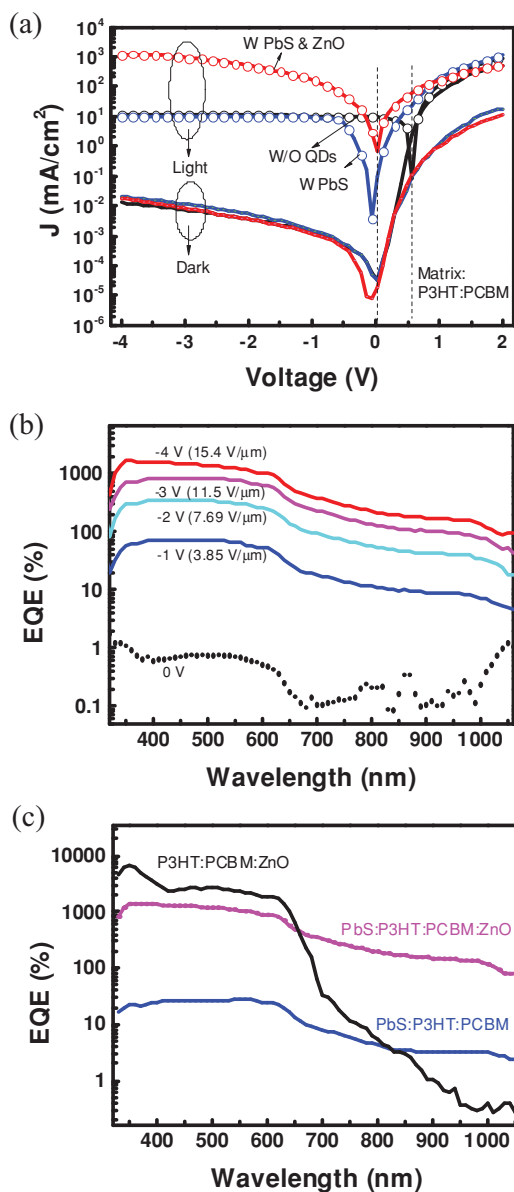

Figure 2. a) Photo- and dark-current density (J)–voltage (V) curves of the P3HT:PCBM, PbS:P3HT:PCBM, and PbS:P3HT:PCBM:ZnO devices; b) EQEs of the PbS:P3HT:PCBM:ZnO device under reverse biases; c) EQEs of the PbS:P3HT:PCBM, ZnO:P3HT:PCBM, and PbS:P3HT:PCBM:ZnO devices at −4 V.

and the results are shown in Figure 2b. The shape of the EQE curves agrees well with that of the absorption spectrum of the quarternary blend film (Figure 1b). The EQE of the quarternary blend film device is very low at zero bias while increasing sharply with the increased reverse bias. The EQE exceeds 100% in the UV and visible range at an applied bias of −2 V (7.69 V/μm); in the NIR range a larger reverse bias of −3 V (11.5 V/μm) is needed because of the lower absorption in this range. The sharp increase of EQE versus bias is consistent with the rapid increase of photocurrent, as shown in Figure 2a. At a bias of −4 V (15.4 V/μm), the EQE values are 1,624%, 1,391%, and 166% at 350 nm, 500 nm, and 930 nm, respectively. Although

www.MaterialsViews.com

ADVANCED
OPTICAL
MATERIALS
www.advopticalmat.de

COMMUNICATION

the thickness of device active layer varied compared with PbS NIR detectors,[17,20,22] the present and reported devices have a very similar working electric field strength. The corresponding responsivity (R in A/W), which is the ratio of photocurrent density to the intensity of incident light, could be calculated from the EQE to be 4.58 A/W, 5.60 A/W, and 1.24 A/W, respectively. These values are much higher than those of commercial SiC, Si, and InAsGa photodetectors. In particular, the huge improvement of responsivity in the NIR range after the integrating of ZnO QDs can be seen from Figure 2c. The EQE of the PbS:P3HT:PCBM device remains below 100% even at the same large reverse bias. Compared with PbS:P3HT:PCBM ternary blend film device, the EQE value in the NIR range of the dual-QD photodetector increases by almost one order of magnitude.

The observed higher photocurrent and EQE suggest that the incorporation of ZnO QDs has a significant influence on the charge injection and the transportation of charge carriers generated by incident photons. In order to find out the detailed mechanism, we first examined the energy diagram of the ternanry and quaternary material systems, as shown in **Figure 3**a,b. As can be seen from both energy diagrams, photogenerated electrons and holes in PbS QDs can be transferred to and transported by PCBM and P3HT, where PbS QDs work as sentitizers for the NIR response, as observed previously by Jarzab et al.[29] Because of the energy level difference, a large injection barrier exists between the Al electrode and the highest occupied molecular orbital (HOMO) of PbS QDs, P3HT, and PCBM. The energy diagram supports the conclusion that the ternary blend film devices are in photodiode mode and have no internal gain. In the quarternary blend film device with doped ZnO QDs, we expect the trapped electrons in ZnO QDs will induce a band bending close to the cathode interface and thus trigger hole injection under reverse bias, which is the origin of the gain.[10] The existence of a large density of charge traps in ZnO QDs is confirmed by the photoluminescence (PL) study. The PL spectrum of ZnO QDs shows a broad green emission around 550 nm from a defect emission, which is assgined to the oxygen (V_O) and/or zinc vacancies (V_{Zn}).[30,31] The strong defect PL emission implies a large density of defects in the ZnO QDs formed by the method we used. The ZnO QDs in this work were prepared using a simple hydrolysis method without any additives, so that surface passivation of defects could be avoided.[32] The purpose of such a preparation is to increase the density of defects and their electron trapping ability, which has been proven using previous ZnO QD:P3HT hybrid devices.[10] The doped ZnO QDs can trap electrons generated in P3HT, PCBM, and PbS based on its energy level, shown in Figure 3b. The electron transfer from PbS,P3HT:PCBM polymer matrix to ZnO QDs has also been confirmed by a PL study. As shown in Figure 3c, the PL intensity of PbS QDs decreases sharply by blending ZnO QDs, demonstrating the electron tranfer from PbS to ZnO. The PL emission of ZnO QD defects is also reduced by removing holes on ZnO, leaving long-lifetime trapped electrons on ZnO, which is important for the observed photoconductive gain. Further PL quenching of both ZnO and PbS was observed by adding the P3HT:PCBM matrix, which can be predicted from their energy levels as well. Based on these results and analysis, the device operational principle can be summarized as: incident
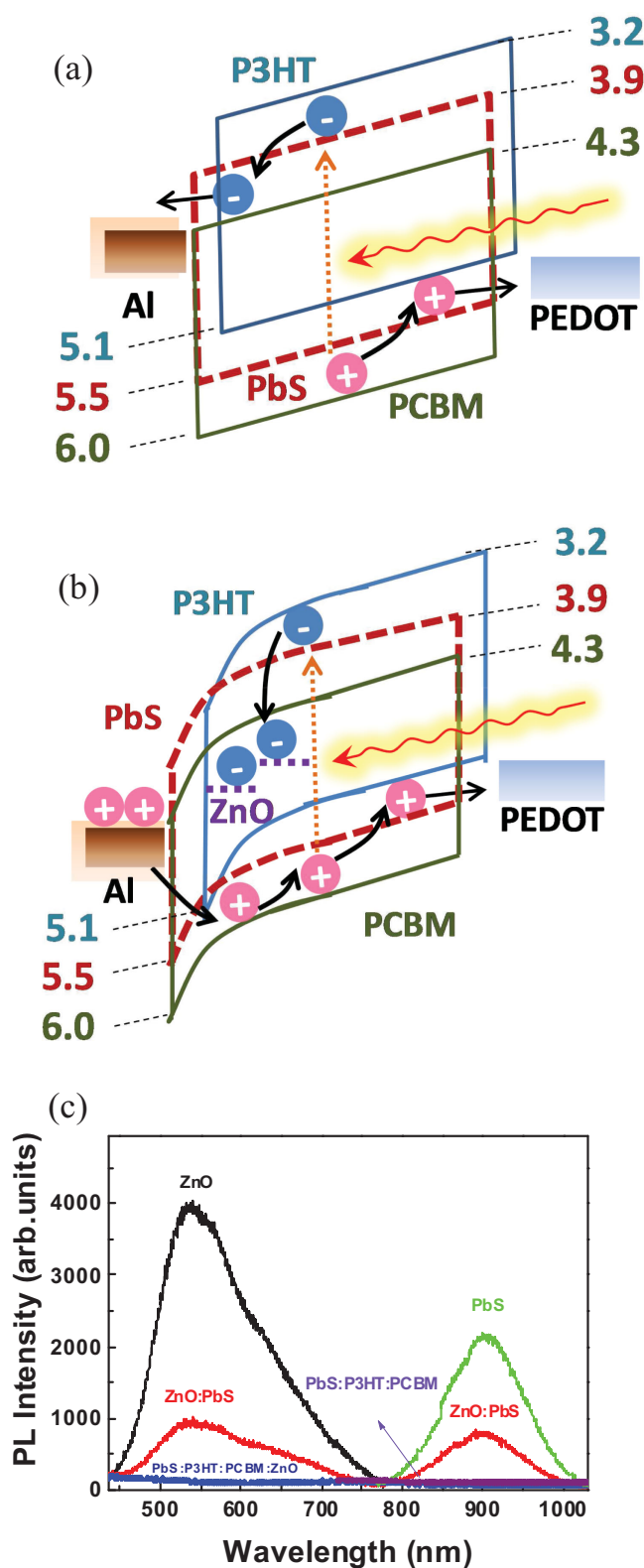

Figure 3. (a,b) Energy diagram of the PbS:P3HT:PCBM ternary blend film photodetector (a) and PbS:P3HT:PCBM:ZnO quaternary blend film photodetector (b) under reverse bias under illumination. PbS QDs: red dashed line, P3HT: blue solid line, PCBM: green solid line, c) PL spectra of ZnO, PbS, PbS:ZnO, PbS:P3HT:PCBM, and PbS:P3HT:PCBM:ZnO films.

**ADVANCED
OPTICAL
MATERIALS**
www.advopticalmat.de

*Materials
Views*
www.MaterialsViews.com

photons absorbed in P3HT, PCBM, ZnO and PbS firstly generate electron–hole pairs, which seperate at the interface of these individual components into free electrons and holes; holes eventually end up on P3HT due to it having the highest HOMO among all these components, and electrons end up trapped by ZnO due to it having the lowest LUMO and trap state energy levels; the trapped electrons near the cathode side cause a large band bending, which dramatically reduces the hole injection barrier from the Al cathode under reverse bias; since one trapped electron can trigger the injection of multiple holes from the cathode, there is apparent gain in the devices with incorporated ZnO QDs. The trapped electrons in ZnO QDs, which are photogenerated on and transfered from P3HT, PCBM, and PbS QDs, cause the observed gain in the whole spectrum from UV to NIR. Moreover, the EQE values in the UV and visible regime decrease after the addition of PbS QDs into the P3HT:PCBM:ZnO device (Figure 2c), which can be attributed to the dilution of ZnO QD density close to the cathode. Part of the incident visible light might be absorbed by the PbS QDs, which have a lower photon-to-current conversion efficiency. It should be noted that the electron transfer from PbS to ZnO, either direct transfer or indirect transfer through PCBM, is paramount for the observed gain in the NIR range.

Photodiodes have low noise but no gain unless a large bias is applied for carrier avalanche. Photoconductors can have higher gain, but usually have large noise currents because an ohmic contant is needed to provide sufficient charge injection. The present dual-QD hybrid photodetector acts as a photodiode in the dark with a rectifying behavior and as a photoconductor under illumination with an ohmic conduction, as shown in the J–V curve (Figure 2a). Therefore, dual-QD hybrid photodetector combines the merits of low noise of the photodiode and large gain of the photoconductor, which should give a high sensitivity value. Specific detectivity (D*) is the parameter to evalute the performance of photodetectors, which is independent of the device area.[33,34] The specific detectivity is determined by

$$D^* = \frac{(AB)^{1/2}}{NEP} \, (\mathrm{cmHz}^{1/2}\,\mathrm{W}^{-1} \, \mathrm{or} \, \mathrm{Jones}) \qquad (1)$$

$$NEP = \frac{\overline{I_n^2}^{1/2}}{R} \, (\mathrm{W}) \qquad (2)$$

where A is the active area of device, B is the bandwidth, NEP is noise equivalent power (defined as the minimal optical signal for the signal-to-noise ratio to be unity), $\overline{I_n^2}^{1/2}$ is the total noise which consists of mainly shot noise (dark current noise) and 1/f noise. The total noise current of the dual-QD hybrid photodetector was directly measured with an SR830 lock-in amplifier under different conditions of dark current density and frequency.[5] As shown in **Figure 4**a and its inset, the measured total noise current was found to be dominated by the shot noise within the frequency range from 1 Hz to 10 kHz. The specific detectivity of the dual-QD photodetector was calculated with responsivity, device area, bandwidth, and measured noise
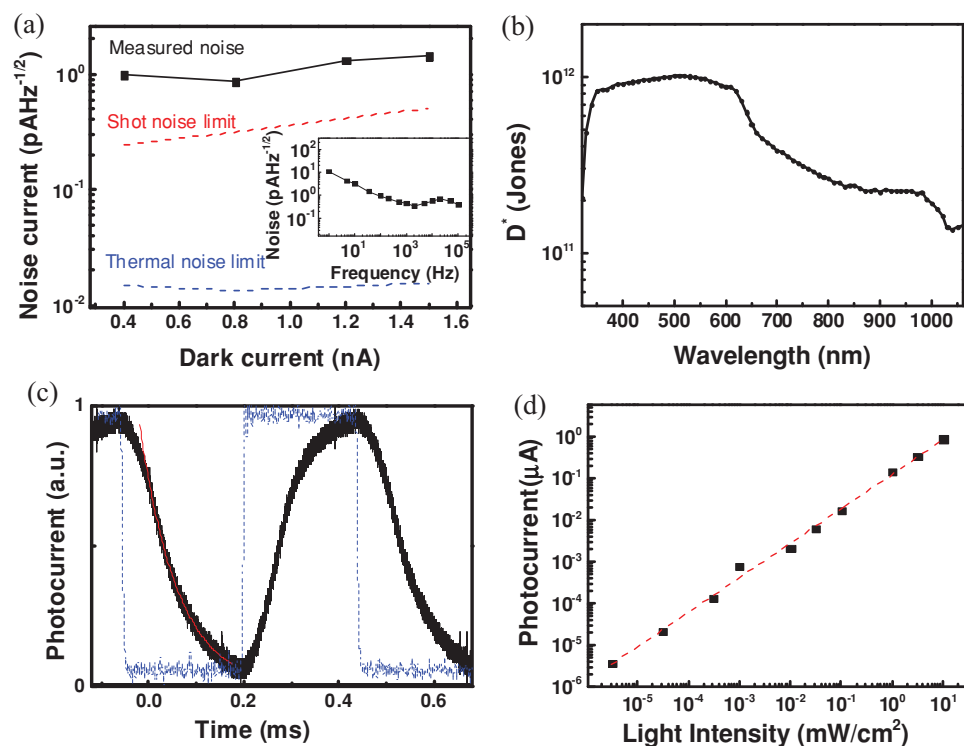

Figure 4. a) The measured noise of the PbS:P3HT:PCBM:ZnO photodetector. The shot noise and thermal noise limits are also shown. Inset: The frequency-dependent noise current measured at −3 V. b) Specific detectivity of the dual-QD photodetector at different wavelengths. c) Transient photocurrent of the PbS:P3HT:PCBM:ZnO photodetector measured at −3 V with a light intensity of 0.1 mWcm⁻²; the dotted line shows the time response of mechanical chopping calibrated by a commercial silicon photodiode. d) Light intensity-dependent photocurrent output.

www.MaterialsViews.com

ADVANCED
OPTICAL
MATERIALS

www.advopticalmat.de

COMMUNICATION

Table 1. The responsivity, NEP, D* of the PbS:P3HT:PCBM:ZnO photo-detector at three selected wavelengths of UV, visible, and NIR.

	350 nm	500 nm	930 nm
Responsivity [A/W]	4.58	5.60	1.24
NEP [pW]	0.314	0.256	1.15
Detectivity* [cmHz$^{1/2}$W^{-1}]	8.28×10^{11}	1.01×10^{12}	2.26×10^{11}

current, as shown in Figure 4b. The values of responsivity, NEP, and D* of the dual-QD hybrid photodetector at three specific wavelengths have been listed in **Table 1**. The responsivity and D* of the dual-QD photodetector is much higher than that of the existing PbS:P3HT:PCBM photodetector.

The ability to quickly detect light is also a crucial parameter for evaluating the performance of photodetectors. It has been previously proven by us that the temporal response of a ZnO (UV) and P3HT (visible) nanocomposite photodetector is among the highest in any QD- or nanoparticle-based photodetector.[10] Here, the NIR response speed of the dual-QD hybrid photodetector was characterized by a chopper controlled laser pulse (808 nm). Figure 4c shows the transient photocurrent of the hybrid device measured under a bias of −3 V at a light intensity of 0.1 mW/cm^2. The transient response result shows a rise time (output signal changing from 10% to 90% of the peak output value) of 160 µs. The decay of the photocurrent after switching off the NIR pulse is around 80 µs. The rise of photocurrent involves multiple steps of time response such as photon absorption, electron–hole pair separation, electron/hole diffusion and trapping, trapping-induced band bending near the cathode, and hole injection. Among these steps, the time needed for trapped electrons to reach saturation concentration may dominate device rise time. In the case of the incident light being turned off, the opposite carrier recombination process will determine the fall time. A linear dynamic range (LDR) is defined as the response range of the detector being linear, where the output current or voltage signal is linearly proportional to its input optical signal.[33,34] In LDR, the waveform of an input optical signal faithfully converts to an output electrical signal without distortion. The LDR of the dual-QD photodetector at NIR wavelength (808 nm) was characterized by measuring the photocurrent at a fixed frequency of 35 Hz with varied light intensity, and the result is shown in Figure 4d. The dual-QD hybrid shows a LDR of 70 dB from 10 mW/cm^2 to 3.1 nW/cm^2. To our knowledge, this is among the best LDR among all polymer and/or QDs based NIR photodetector.[2,19] It should be pointed out that the illumination intensity has an influence on the trap filling, band bending, and charge injection so that the EQE value will decrease when the light is sufficiently low, i.e., a decrease has already been observed in our previous UV detector[10] which processes a similar working mechanism.

In summary, we reported a dual-QD hybrid photodetector which is a photodiode in the dark with a rectifying behavior and is a photoconductor under illumination with an ohmic conduction. With the incorporation of ZnO QDs, a gain in NIR range is introduced in the QD hybrid photodetectors. The EQE in the NIR wavelength was higher than 100% and the responsivity is much higher than that of the PbS:P3HT:PCBM photodetectors. It should be noted that PbS QD-based photo-detectors have been widely studied over the past decade, while most of the previous efforts were focused on reducing the inter-QD distance, for example, by substituting the long ligands to shorter ligands in the solid phase so that a better carrier transport ability is achieved. However, such an active layer deposition and ligands exchange processes are relatively complicated and multiple layer deposition with tens of precision cycles is required. In contrast to those photodetectors, our dual-QD hybrid photodetectors are much simpler to fabricate using a single spin-coating step. The reported high sensitivity, low cost, and room temperature-operated dual-QD hybrid photodetector should have great potential to find applications in a wide range of fields.

Experimental Section

Quantum Dots and Polymer Solutions: The PbS QDs were synthesized and capped with butylamine as described in the literature.[21–23] Bis(trimethylsilylsulphide) was injected into a nitrogen-protected reaction flask containing lead oxide, oleic acid, and octadecene, then oleate-capped PbS QDs were precipitated with acetone and re-dissolved in toluene twice to isolate the QDs. After being precipitated with methanol and re-dissolved in toluene twice, the oleate-capped PbS QDs were re-dissolved in butylamine for solution-phase ligand exchanging, and then the PbS QDs were precipitated again with isopropanol and dissolved in DCB to make a 70 mg/mL solution (PbS solution). ZnO QDs were prepared using a hydrolysis method in methanol.[24–26] Zinc acetate was dissolved in methanol and followed by adding potassium hydroxide solution. After the reaction solution became turbid, ZnO QDs were collected by centrifuge and washed with methanol three times. ZnO QDs were dissolved in DCB to make a 70 mg/mL solution, and then 5% (vol) butylamine was added into the ZnO QD solution (ZnO solution). P3HT and PCBM were dissolved in DCB to make a 35 mg/mL solution (polymer solution). The ZnO solution and polymer solutions were mixed with a volume ratio of 1:1 (ZnO:Polymer blend). The PbS solution and polymer solution were mixed with a volume ratio of 2:1 (PbS:Polymer blend). The ZnO:Polymer blend and PbS:Polymer blend were then mixed with a volume ratio of 1:1:1 (ZnO:PbS:Polymer blend).

Device Fabrication: Poly(3,4-ethylenedioxythiophene) poly(styrene-sulphonate) (PEDOT:PSS) was first spin-coated onto a cleaned ITO/glass substrate at a spin speed of 3000 r.p.m., which gives a PEDOT:PSS film thickness of approximately 30 nm. The PEDOT:PSS was then baked at 120 °C for 30 min. The as-prepared ZnO–PbS–Polymer blends were spin-coated at 600 r.p.m. for 90 s, then solvent annealed for 8 hours by placing the devices in the vapor of the solvent DCB, which significantly slows down the drying of the polymers. Thermal annealing was performed at 110 °C for 15 min before the evaporation of metal contacts. The thicknesses of the active layers were around 200–300 nm. A 100 nm thick aluminium was thermally evaporated on to the photoactive layer as the cathode. The active device area was around 0.06 cm^2, defined by the shadow masks.

Device Characterization: EQE was measured with a Newport QE measurement kit by focusing a monochromatic beam of light onto the devices. For the transient response measurement, an optical chopper was used to provide the light pulse, and an oscilloscope (LeCroy WaveRunner) was used to record the voltage variation of the resistor. The absorption spectra of the photoactive layers were measured with an Evolution 210 spectrometer. In order to have an accurate UV absorbance value, the device was prepared on a quartz substrate. Photoluminescence measurements were performed with a Horiba 320 detector. Film thickness was measured with an AMBIOS XP-2 stylus profilometer. Noise current was directly measured with a lock-in amplifier SR830.

Acknowledgements

[1] X. Gong, M. Tong, Y. Xia, W. Cai, J. S. Moon, Y. Cao, G. Yu, C.-L. Shieh, B. Nilsson, A. J. Heeger, *Science* **2009**, *325*, 1665.

[2] G. Konstantatos, E. H. Sargent, *Nat. Nanotechnol.* **2010**, *5*, 391.

[3] J. Tang, E. H. Sargent, *Adv. Mater.* **2011**, *23*, 12.

[4] K.-J. Baeg, M. Binda, D. Natali, M. Caironi, Y.-Y. Noh, *Adv. Mater.* **2013**, *25*, 4267.

[5] H. Y. Chen, M. K. F. Lo, G. W. Yang, H. G. Monbouquette, Y. Yang, *Nat. Nanotechnol.* **2008**, *3*, 543.

[6] T. K. An, C. E. Park, D. S. Chung, *Appl. Phys. Lett.* **2013**, *102*, 193306.

[7] S. T. Chuang, S. C. Chien, F. C. Chen, *Appl. Phys. Lett.* **2012**, *100*, 013309.

[8] F. C. Chen, S. C. Chien, G. L. Cious, *Appl. Phys. Lett.* **2010**, *97*, 103301.

[9] M. He, J. Ge, Z. Q. Lin, X. H. Feng, X. W. Wang, H. B. Lu, Y. L. Yang, F. Qiu, *Energy Environ. Sci.* **2012**, *5*, 8351.

[10] F. W. Guo, B. Yang, Y. B. Yuan, Z. G. Xiao, Q. F. Dong, Y. Bi, J. S. Huang, *Nat. Nanotechnol.* **2012**, *7*, 798.

[11] A. Gocalinska, M. Saba, F. Quochi, M. Marceddu, K. Szendrei, J. Gao, M. A. Loi, M. Yarema, R. Seyrkammer, W. Heiss, A. Mura, G. Bongiovanni, *J. Phys. Chem. Lett.* **2010**, *1*, 1149.

[12] M. He, F. Qiu, Z. Q. Lin, *J. Phys. Chem. Lett.* **2013**, *4*, 1788.

[13] M. He, F. Qiu, Z. Q. Lin, *Energy Environ. Sci.* **2013**, *6*, 1352.

[14] D. V. Talapin, J. S. Lee, M. V. Kovalenko, E. V. Shevchenko, *Chem. Rev.* **2010**, *110*, 389.

[15] G. Konstantatos, I. Howard, A. Fischer, S. Hoogland, J. Clifford, E. Klem, L. Levina, E. H. Sargent, *Nature* **2006**, *442*, 180.

[16] R. Saran, M. N. Nordin, R. J. Curry, *Adv. Funct. Mater.* **2013**, *23*, 4149.

[17] J. P. Clifford, G. Konstantatos, K. W. Johnston, S. Hoogland, L. Levina, E. H. Sargent, *Nat. Nanotechnol.* **2009**, *4*, 40.

[18] G. Konstantatos, J. Clifford, L. Levina, E. H. Sargent, *Nat. Photonics* **2007**, *1*, 531.

[19] T. Rauch, M. Böberl, S. Tedde, J. Fürst, M. V. Kovalenko, G. Hesser, U. Lemmer, W. Heiss, O. Hayden, *Nat. Photonics* **2009**, *3*, 332.

[20] G. Itskos, A. Othonos, T. Rauch, S. F. Tedde, O. Hayden, M. V. Kovalenko, W. Heiss, S. A. Choulis, *Adv. Energy Mater.* **2011**, *1*, 802.

[21] M. A. Hines, G. D. Scholes, *Adv. Mater.* **2003**, *15*, 1844.

[22] K. Szendrei, F. Cordella, M. V. Kovalenko, M. Böberl, G. Hesser, M. Yarema, D. Jarzab, O. V. Mikhnenko, A. Gocalinska, M. Saba, F. Quochi, A. Mura, G. Bongiovanni, P. W. M. Blom, W. Heiss, M. A. Loi, *Adv. Mater.* **2009**, *21*, 683.

[23] F. W. Wise, *Acc. Chem. Res.* **2000**, *33*, 773–780.

[24] C. Pacholski, A. Kornowski, H. Weller, *Angew. Chem. Int. Ed.* **2002**, *41*, 1188.

[25] W. J. E. Beek, M. M. Wienk, R. A. J. Janssen, *Adv. Mater* **2004**, *16*, 1009.

[26] B. Q. Sun, H. Sirringhaus, *Nano Lett.* **2005**, *5*, 2408.

[27] G. Li, V. Shrotriya, J. S. Huang, Y. Yao, T. Moriarty, K. Emery, Y. Yang, *Nat. Mater.* **2005**, *4*, 864.

[28] W. Ma, C. Yang, X. Gong, K. Lee, A. J. Heeger, *Adv. Funct. Mater.* **2005**, *15*, 1617.

[29] D. Jarzab, K. Szendrei, M. Yarema, S. Pichler, W. Heiss, M. A. Loi, *Adv. Funct. Mater.* **2011**, *21*, 1988.

[30] V. A. Fonoberov, K. A. Alim, A. A. Balandin, F. X. Xiu, J. L. Liu, *Phys. Rev. B* **2006**, *73*, 165317.

[31] S. Mahamuni, K. Borgohain, B. S. Bendre, V. J. Leppert, S. H. Risbud, *J. Appl. Phys.* **1999**, *85*, 2861.

[32] C. L. Yang, J. N. Wang, W. K. Ge, L. Guo, S. H. Yang, D. Z. Shen, *J. Appl. Phys.* **2001**, *90*, 4489.

[33] J. M. Liu, *Photonic Devices* Cambridge Univ. Press, New York **2005**, p. 940.

[34] S. M. Sze, K. K. Ng, *Physics of Semiconductor Devices* Wiley-Interscience, New Jersey **2007**, p. 663.